

The logo for EPJ B is a dark blue rectangle. The left side of the rectangle is a vertical strip with a red and orange abstract pattern. The text "EPJ B" is written in a white, serif font in the center of the blue area.

EPJ B

www.epj.org

Condensed Matter
and Complex Systems

Eur. Phys. J. B **64**, 271–276 (2008)

DOI: 10.1140/epjb/e2008-00311-x

Initial growth of the Rayleigh-Taylor instability via molecular dynamics

J.L. Barber, K. Kadau, T.C. Germann and B.J. Alder



Initial growth of the Rayleigh-Taylor instability via molecular dynamics

J.L. Barber^{1,a}, K. Kadau¹, T.C. Germann¹, and B.J. Alder²

¹ Los Alamos National Laboratory - Los Alamos, New Mexico 87545, USA

² Lawrence Livermore National Laboratory - Livermore, California 94550, USA

Received 25 March 2008 / Received in final form 9 June 2008

Published online 30 July 2008 – © EDP Sciences, Società Italiana di Fisica, Springer-Verlag 2008

Abstract. At small length scales, the fluctuations that are neglected in most continuum descriptions of fluids become important. In this work, we explore the emergence of the Navier-Stokes equations as the ensemble mean of these fluctuations, which are inherent in the fundamental molecular processes underlying a fluid. This is accomplished by examining the initial growth of the Rayleigh-Taylor instability via hundreds of large-scale molecular dynamics simulations. A comparison of the mean growth rate spectra with the corresponding continuum predictions yields good agreement over a range of length scales from $\sim 1 \mu\text{m}$ to as small as $\sim 10 \text{ nm}$. However, individual simulations exhibit significant variations from the continuum prediction. This work helps pave the way to a more fundamental understanding of fluid dynamics on small scales, and the mechanisms by which macroscopic, continuum models emerge. Such an understanding is essential, for example, in the rapidly growing field of nanotechnology.

PACS. 47.20.Ma Interfacial instabilities – 02.70.Ns Molecular dynamics and particle methods

1 Introduction

Continuum models, such as the Navier-Stokes (NS) equations, have been generally successful in describing various aspects of fluid flow. However, the validity of the NS equations at the macroscopic level is an emergent phenomenon of the molecular dynamics underlying the fluid. Furthermore, in the microscopic regime corrections to the NS equations must be made due to fluctuations [1] and, in the presence of strong gradients, nonlinear transport effects [2]. For low-gradient systems, the NS equations emerge as the ensemble mean over the fluctuations inherent at small scales [3], although particular instances of the flow at such scales may exhibit large deviations from NS-like behavior. In practice, there exists a boundary in parameter space which delineates the circumstances under which a purely deterministic, continuum fluid model is valid. In this work we explore this boundary in the context of the Rayleigh-Taylor instability (RTI) (Fig. 1). However, our results have a wider, qualitative applicability to fluid behavior at the nanoscale, particularly for non-stationary flows, and to the relationship between micro- and macroscale models.

The emergence of continuum models from their atomistic antecedents has been explored before in the literature [4,5], usually by comparing flows generated by the NS equations with the results of simulations using atom-



Fig. 1. Time series of images from a $g = 1.3 \times 10^{10} g_{Earth}$ simulation of the RTI. Red is the heavy fluid; blue is the light fluid. Dashed line: reference sine curve corresponding to the predicted wavenumber of maximum instability k_m .

istic models such as molecular dynamics (MD) [6,7], in which the classical equations of motion for a large system of interacting molecules are solved numerically. Remarkable agreement has been found, even in surprisingly small MD systems. However, most previous work has concentrated on stationary flows, in which the possibility of time-averaging the solution yields a significant reduction in systematic noise. While this allows for a simpler comparison with continuum results, it obscures the fluctuations that are fundamental to the nature of fluids at small scales. For this reason we focus on a complex, non-stationary flow, enabling us to determine the relative magnitude of fluctuations at various scales.

^a e-mail: jlbarber@lanl.gov

The RTI [8,9] occurs when a heavy fluid lies on top of a light fluid in the presence of gravity. This arrangement is unstable, and the two fluids subsequently combine in an archetypical example of turbulent fluid mixing. The details of the well-developed, turbulent stage of the RTI have been studied extensively via both experiment and simulation [10]. The majority of the simulations to date have been performed using traditional continuum codes, i.e. NS solvers of various types. In principle, however, it is desirable to investigate complex flows through more fundamental atomistic methods, especially at small scales, and there have been recent efforts to study the RTI using MD [11] and other atomistic methods [12]. It is our goal in this work to explore the emergence of the NS equations in the linearized regime by examining the initial growth of the fluid interface in the RTI using MD, and comparing the results with existing continuum linear stability theory. One major advantage of using MD is the ability to start with an essentially flat interface, which is perturbed only by an extremely small roughness on the order of the size of a molecule. This is generally impossible in continuum simulations, since a perfectly flat interface without perturbations is an unstable equilibrium which will persist forever in a deterministic simulation using a traditional NS solver. In order for the interface to become unstable and exhibit interesting behavior in a reasonable period of time, an artificial and somewhat arbitrary spectrum of perturbations must be imposed on the interface at $t = 0$. Recent continuum simulation results suggest that the subsequent dynamics of the instability may depend strongly on the details of this initial spectrum [12]. In experiments, for various practical reasons relating to experimental design, a flat interface is achievable only with great difficulty [13].

After outlining the relevant linear stability theory and describing our simulation and data analysis techniques, we offer an interpretation of the results.

2 Linear stability analysis

Consider a heavy fluid of density ρ_h and kinematic viscosity ν_h on top of a light fluid of density ρ_ℓ and kinematic viscosity ν_ℓ . The two fluids are initially separated by a flat, horizontal interface at $z = 0$. Here z is the vertical coordinate, whereas x and y are the coordinates parallel to the initial plane of the interface. To explore the stability of this arrangement via linear stability analysis, we examine the behavior of small perturbations in the velocity and density fields whose dependence on x , y , and time t takes the form $\exp(nt + ik_x x + ik_y y)$, where (k_x, k_y) is the wavevector of the perturbation, and n is the corresponding growth rate, which in general may be complex. Harrison [14] and Chandrasekhar [15] have shown that if the system is governed by the incompressible NS equations,

$$\begin{cases} \partial_t \rho + \nabla \cdot (\rho \mathbf{u}) = 0 \\ \partial_t \mathbf{u} + (\mathbf{u} \cdot \nabla) \mathbf{u} = -\frac{1}{\rho} \nabla p + \nu \Delta \mathbf{u} + \mathbf{g} \\ \nabla \cdot \mathbf{u} = 0, \end{cases} \quad (1)$$

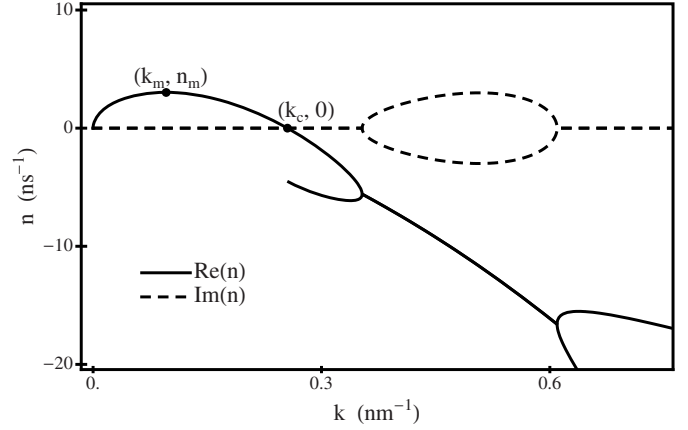


Fig. 2. Real and complex branches of $n(k)$ as predicted by linear stability analysis via the numerical solution of equation (2), for the set of material properties used in all of our MD simulations and $g = 2.7 \times 10^{10} g_{Earth}$.

then n and $k \equiv (k_x^2 + k_y^2)^{1/2}$ are implicitly related via

$$\begin{aligned} f(k, n) \equiv & - \left(\frac{k}{n^2} \left[\frac{\gamma k^2}{(\rho_\ell + \rho_h)} - Ag \right] + 1 \right) \left(\frac{\rho_h q_\ell + \rho_\ell q_h}{\rho_\ell + \rho_h} - k \right) \\ & + \frac{4\bar{\nu} k^2}{n} \left(\frac{\rho_h q_\ell - \rho_\ell q_h}{\rho_\ell + \rho_h} - Ak \right) \\ & - 4 \frac{\rho_\ell \rho_h k}{(\rho_\ell + \rho_h)^2} + \frac{4\bar{\nu}^2 k^3}{n^2} (q_\ell - k)(q_h - k) = 0, \end{aligned} \quad (2)$$

where $q_{\ell,h} \equiv \sqrt{k^2 + n/\nu_{\ell,h}}$, $\bar{\nu} \equiv (\rho_\ell \nu_\ell - \rho_h \nu_h)/(\rho_\ell + \rho_h)$, $\rho_h(\rho_\ell)$ is the mass density of the heavy (light) fluid, $A \equiv (\rho_h - \rho_\ell)/(\rho_h + \rho_\ell)$ is the Atwood number, $g = |\mathbf{g}|$ is the acceleration due to gravity, and γ is the interfacial tension.

Given values for the material properties ρ_h , ρ_ℓ , ν_h , ν_ℓ , and γ , as well as the gravity g , equation (2) can be solved numerically to yield n as a function of k . In general, there may be more than one branch of complex solutions. As an example, the results of such a numerical solution are shown in Figure 2. This solution corresponds to the set of material properties used in all of our MD simulations (see below), as well as to the highest gravity we used in this work ($g = 2.7 \times 10^{10} g_{Earth}$, where g_{Earth} is the Earth's acceleration due to gravity). Depending on the value of k , there may be one real solution with $n(k) > 0$, two real solutions with $n(k) < 0$, or two complex-conjugate solutions with $\text{Re}(n(k)) < 0$. In either experiment or in any type of RTI simulation, we expect the growth rate of the interface at every value of k to be dominated by the branch of $n(k)$ with the largest real part.

The results shown in Figure 2 are qualitatively representative of any of the gravities we considered, in that the overall shape of the $n(k)$ curves is the same for any of our g values, though the precise numerical details may vary. Note the existence of a wavenumber of maximum instability (i.e. with maximal n), and a cutoff wavenumber, above which modes are damped (i.e. $\text{Re}(n(k)) < 0$).

These special values of k will be denoted by k_m and k_c , respectively. By considering the energetic interplay between interfacial tension and gravity, it can be shown that $k_c = [g(\rho_h - \rho_\ell)/\gamma]^{1/2}$ [15]. We are aware of no similar analytical expression for k_m . In general, the magnitude of the growth rate is a decreasing function of interfacial tension and viscosity.

3 Simulations

Previous work on the initial growth of the RTI [11] treated the problem only in passing, did not include any discussion of the emergence of continuum models, and included a far smaller number of simulations, which focused on single-mode imposed perturbations for one value of g . Here, in order to generate growth rate data for comparison with the continuum prediction, we have performed hundreds of large-scale MD simulations at several values of g . These simulations contained heavy and light particles, initially separated by a flat interface which subsequently roughened due to thermal fluctuations [16]. In the linear-growth regime, each mode evolved independently and each simulation simultaneously provided information about all the modes of interest.

Our heavy-heavy and light-light interaction potentials were based on a splined version of the Lennard-Jones potential

$$u(r) = \varepsilon \left[\left(\frac{r_0}{r} \right)^{12} - 2 \left(\frac{r_0}{r} \right)^6 \right]. \quad (3)$$

To ensure immiscibility between the two fluids, only the repulsive part of the Lennard-Jones potential was used as the heavy-light interaction potential. For further details on the nature of the splined potentials used, see [11].

Our MD simulations were performed using a dimensionless system of units in which all quantities were expressed in terms of various combinations of r_0 , ε , m_ℓ (the mass of the light species), and k_b (Boltzmann's constant). To approximately convert the simulation results into real units, we have used the values of r_0 , ε , and m_ℓ corresponding to methanol: $r_0 = 4.02 \times 10^{-10}$ m, $m_\ell = 5.31 \times 10^{-26}$ kg, and $\varepsilon = 7.00 \times 10^{-21}$ J [17]. Note that this is not meant to imply that our fluid accurately represents methanol, for which the Lennard-Jones potential is far too simplistic a model. In these units, the initial temperature and number density at the interface were $T = 1.3 \varepsilon/k_b = 660$ K and $n_0 = 0.765/r_0^3 = 1.2 \times 10^{28}$ m $^{-3}$, respectively. The heavy species mass was $7m_\ell = 37.2 \times 10^{-26}$ kg, so that the Atwood number $A = 0.75$. The kinematic viscosities $\nu_\ell = 1.25 \sqrt{\varepsilon r_0^2/m_\ell} = 1.8 \times 10^{-7}$ m 2 /s and $\nu_h = 0.47 \sqrt{\varepsilon r_0^2/m_\ell} = 0.69 \times 10^{-7}$ m 2 /s, as well as the interfacial tension $\gamma = 0.359 \varepsilon/r_0^2 = 1.6 \times 10^{-2}$ J/m 2 , were calculated in separate equilibrium simulations [11]. At such small length scales, the acceleration due to gravity must be very high in order for the instability to develop in a reasonable amount of time. The three gravities considered were therefore $g = 0.0008 \varepsilon/m_\ell r_0 = 2.7 \times 10^{10} g_{Earth}$,

$0.0004 \varepsilon/m_\ell r_0 = 1.3 \times 10^{10} g_{Earth}$, and $0.0001 \varepsilon/m_\ell r_0 = 0.3 \times 10^{10} g_{Earth}$.

In order for any fluid system to display a classical instability, the initial state at $t = 0$ must be an unstable equilibrium. For an incompressible fluid in the Rayleigh-Taylor configuration, this consists of a uniform velocity field $\mathbf{u} = 0$ and a uniform temperature T throughout the domain, as well as an initially piecewise-constant mass density profile in the vertical direction:

$$\rho(z) = \begin{cases} \rho_h & z > 0 \\ \rho_\ell & z < 0. \end{cases} \quad (4)$$

However, compressibility can never be entirely eliminated in an MD simulation, and the mass density profile $\rho(z)$ must be precompressed somewhat in order to achieve hydrostatic equilibrium and to avoid spurious oscillations of the interface. This was accomplished by using an initial number density profile $n(z)$ that satisfied

$$\frac{dn}{dz} \frac{\partial}{\partial n} p(n, T) = \begin{cases} -g \rho_h n & z > 0 \\ -g \rho_\ell n & z < 0. \end{cases} \quad (5)$$

Here $p(n, T)$ is the equation of state associated with the Lennard-Jones potential (Eq. (3)), which was calculated numerically in a separate equilibrium MD simulation [11]. Solving equation (5) numerically subject to the initial condition $n(0) = n_0$ yielded a slowly-varying number density profile that differed from the interface value of n_0 by less than 2 percent at the top and bottom of the domain. This number density profile was then used to generate suitable initial positions for all of the particles in the system. Particles were placed on a randomized cubic lattice, where the average lattice spacing in the vertical direction was increased with increasing height, in accord with the desired profile $n(z)$. Initial velocities for each particle were selected from the appropriate Boltzmann distribution at the given temperature T .

Each simulation contained about 2 000 000 particles each of the heavy and light species. The timestep was $\Delta t = 0.01 \sqrt{m_\ell r_0^2/\varepsilon} = 11$ fs. The total simulation times varied somewhat, but were generally of the order $\sim 3 \times 10^5 \Delta t \sim 3$ ns. We used the Verlet integration method in the NVE ensemble. Although no thermostat was employed, the maximum temperature variation anywhere in the domain in any of the simulations was less than 5 percent. All simulations had domain dimensions of approximately $5r_0 \times 2800r_0 \times 386r_0 = 2.0$ nm \times 1.1 μ m \times 0.16 μ m. There were two reasons for this ‘‘quasi-2D’’ (or ‘‘thin slab’’) geometry. First, performing a sufficient number of fully 3D simulations would have required prohibitively large computational effort. Recall also that in a truly 2D molecular system all transport coefficients, such as the viscosity or diffusivity, diverge. In a quasi-2D geometry, these quantities are all finite, and the result is comparable to a 2D continuum simulation.

At such small scales, the evolution of the fields that characterize the fluid (velocity, mass density, etc.) displays large fluctuations, which result from both the random

initial configuration of particles and their subsequent Brownian motion. It is therefore the ensemble-mean behavior of the linear growth rates that interests us. In order to obtain an acceptable mean, many simulations were performed for each of the three g values considered: 107, 116, and 13 runs for the high, medium, and low gravities, respectively. (The small number of runs in the low-gravity case is due to the much slower development of the interface.) All simulations were performed using the Scalable Parallel Short-range Molecular dynamics code (SPaSM) [18,19]. The Los Alamos National Laboratory high-performance computing clusters used were Coyote (2580 \times AMD Opteron @ 2.6 GHz) and Flash (1906 \times AMD Opteron @ 2.0/2.4 GHz). Each simulation took 12–24 h and used anywhere from 64 to 640 processors.

A time series of images from one of the $g = 1.3 \times 10^{10} g_{Earth}$ simulations is shown in Figure 1. Note that the shape of the interface is quickly dominated by modes near $k = k_m$.

4 Data analysis

We determined the shape of the interface in our simulations at regular time intervals by dividing the domain into a number of vertical “columns”. We estimated the interface position in each column as the value of z at which the number fraction of heavy particles passed 0.5. Due to the quasi-2D geometry, our interface was effectively one-dimensional, and could be characterized via the relation

$$z(y, t) = \sum_k [a_k(t) \sin(ky) + b_k(t) \cos(ky)], \quad (6)$$

where y is the coordinate in the wider of the two horizontal directions. Since our simulations did not proceed long enough to leave the linear growth regime, the coefficients $a_k(t)$ and $b_k(t)$ evolved independently for each k , and could be determined at regular time intervals by performing a Fourier transform of the interface.

The Fourier coefficients $a_k(t)$ and $b_k(t)$ are predicted by classical linear stability theory to evolve according to

$$\begin{cases} \frac{d}{dt} a_k(t) = n(k) a_k(t) \\ \frac{d}{dt} b_k(t) = n(k) b_k(t), \end{cases} \quad (7)$$

so that

$$\begin{cases} a_k(t) = a_k(0) e^{n(k)t} \\ b_k(t) = b_k(0) e^{n(k)t}. \end{cases} \quad (8)$$

However, there are a number of problems with the application of equations (7) and (8) to a fluctuation-laden molecular system with an essentially flat initial interface. For such a system we have $a_k(0) = b_k(0) = 0$ for all k . Equation (8) then implies that the interface will remain flat for all time. That this is not the case stems from the influence of fluctuations, which drive the amplitudes of all interfacial modes away from their initial value of zero.

In this context, it is better to use a model for the evolution of the $a_k(t)$ and $b_k(t)$ which takes into account both the fluctuations and hydrodynamically-driven exponential growth. The simplest such modification of equation (7) that can be constructed is the set of stochastic differential equations (SDEs)

$$\begin{cases} \frac{d}{dt} a_k(t) = n(k) a_k(t) + c(k) W_1(k, t) & a_k(0) = 0 \\ \frac{d}{dt} b_k(t) = n(k) b_k(t) + c(k) W_2(k, t) & b_k(0) = 0. \end{cases} \quad (9)$$

Here $c(k)$ is the noise amplitude and the $W_i(k, t)$ are a family of standard white noise process which satisfy

$$\langle W_i(k, t) \rangle = 0 \quad (10)$$

and

$$\langle W_i(k, t) W_j(k', t') \rangle = \delta_{ij} \delta_{kk'} \delta(t - t'). \quad (11)$$

The angled brackets $\langle \dots \rangle$ represent an average over the ensemble of microscopic randomness.

The solution to equation (9) is

$$\begin{cases} a_k(t) = c(k) \int_0^t ds e^{n(k)(t-s)} W_1(k, s) \\ b_k(t) = c(k) \int_0^t ds e^{n(k)(t-s)} W_2(k, s). \end{cases} \quad (12)$$

Given equations (10)–(12), it is straightforward to show that the root mean square amplitude

$$A_k(t) \equiv \langle a_k^2(t) + b_k^2(t) \rangle^{1/2} \quad (13)$$

is predicted to satisfy

$$A_k(t) = \left[\frac{c^2(k)}{n(k)} \left(e^{2n(k)t} - 1 \right) \right]^{1/2}. \quad (14)$$

This captures the expected behavior of the system at both small and large times. For small t ,

$$A_k(t) \rightarrow |c(k)| (2t)^{1/2}. \quad (15)$$

This $t^{1/2}$ power-dependence reflects the fact that the interface is initially dominated by uncorrelated, fluctuation-driven diffusion. For large t ,

$$A_k(t) \rightarrow \begin{cases} \frac{|c(k)|}{n(k)^{1/2}} e^{n(k)t} & n(k) > 0 \\ \frac{|c(k)|}{|n(k)|^{1/2}} & n(k) < 0. \end{cases} \quad (16)$$

We analyzed our data by fitting the square amplitude $a_k^2(t) + b_k^2(t)$ for each k value in each simulation to the expression for $A_k^2(t)$ derived from equation (14), with $n(k)$ and $c(k)$ as the fitting parameters. The resulting collection of $n(k)$ values allowed us to estimate several quantities. The mean growth rate $n(k)$ at each value of k and g was estimated as the mean of all of the fitted $n(k)$ values from all of the runs at that gravity. The standard deviation $\Delta n(k)$

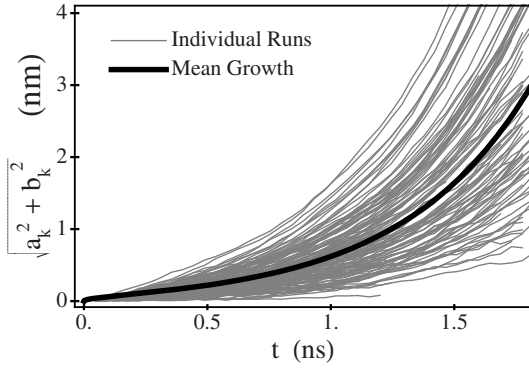


Fig. 3. Individual MD run results for $(a_k(t)^2 + b_k(t)^2)^{1/2}$, as well as the mean fit to equation (14), for $g = 2.7 \times 10^{10} g_{Earth}$ and $k \sim k_m$.

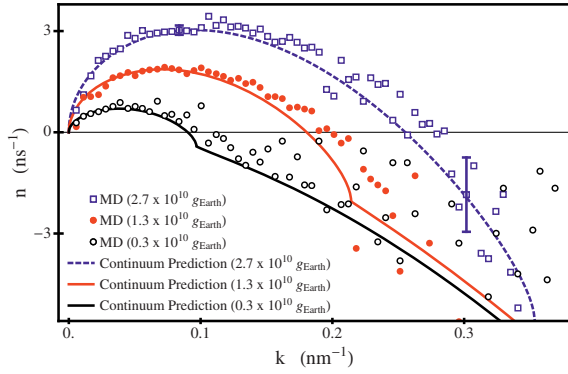


Fig. 4. Mean growth rate data for each gravity, along with the corresponding predictions from continuum linear stability theory. Error bars indicating the uncertainty δn in our estimate of $n(k)$ near k_m and k_c are shown for the highest gravity.

of the fitted growth rate values at wavenumber k is of interest for two reasons. First, the statistical uncertainty in our estimate for $n(k)$ is given by $\delta n(k) = \Delta n(k)/N_r^{1/2}$, where N_r is the number of runs at the corresponding value of g . More importantly, $\Delta n(k)$ provides a measure of the true physical spread in the growth rate at these small length scales.

5 Results

There was a great deal of variability in the amplitude versus time curves even for k near k_c , where we would expect the hydrodynamically-motivated exponential growth to dominate (Fig. 3). This variability is a result of the fact that at these small scales, the growth rate fluctuates a great deal. The magnitude of these fluctuations should become vanishingly small as one approaches the macroscale. It is therefore the mean value of n to which the continuum prediction must be compared. Such a comparison for each of the three gravities considered is shown in Figure 4. For reference, note that the length scales corresponding to k_m and k_c in the medium gravity case are ~ 190 and ~ 80 interatomic spacings, respectively.

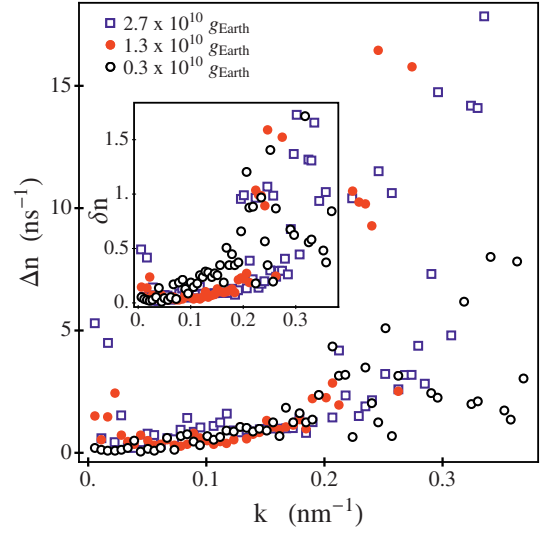


Fig. 5. Inherent physical variability $\Delta n(k)$ in the growth rate. Inset: the corresponding uncertainty $\delta n(k) = \Delta n(k)/(\# \text{ of runs})^{1/2}$ in our estimate of the mean growth rate $n(k)$.

Several points can be made about these results. First of all, despite the fluctuations present in the system, the quantitative agreement is quite good, confirming even the existence of a cutoff wavenumber. However, there is a general tendency for the MD data to lie slightly above the theoretical curve at high k , which may be due to several influences. In our data analysis, we have assumed that n is real. In reality, n may have a nonzero imaginary part (Fig. 2). The associated oscillations, though perhaps not discernable in any one run, may systematically increase the apparent mean growth rate over a short data set. Also neglected is the fact that surface tension and viscosity are k -dependent at small scales. However, such effects are only important at the scale of several molecular diameters [2], and should have little effect at the values of k we are considering. The effects of compressibility – present in MD, but neglected in the linear stability analysis – cannot be the cause of this discrepancy, as it has been shown in [20] that compressibility can only reduce the growth rate. Furthermore, the maximum Mach numbers attained in these simulations were only ~ 0.02 and ~ 0.007 within the heavy and light fluids, respectively, suggesting that compressibility has a marginal effect, if any. (Mach numbers were estimated as the ratio of the rate of progress of the interface divided by the theoretical sound speeds in the two fluids based on the appropriate equation of state.)

The physical variation $\Delta n(k)$ of the growth rate is shown in Figure 5, and the uncertainty $\delta n(k)$ in our estimate of $n(k)$ is given in the inset. As can be seen in the figure, $\Delta n(k)$ is an increasing function of k . (The apparent jump in $\Delta n(k)$ at the lowest values of k is a boundary effect due to the periodicity of our system, and can be ignored.) In particular, for $0.03 \text{ nm}^{-1} < k < 0.2 \text{ nm}^{-1}$, we see that the $\Delta n(k)$ results for all three gravities collapse approximately onto a single increasing curve. This is to be expected, since $\Delta n(k)$ results from the influence

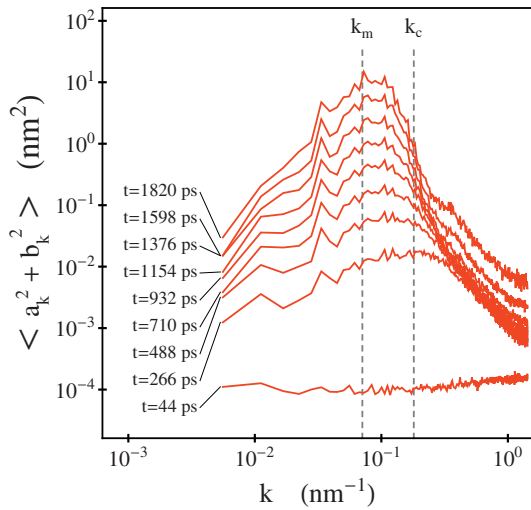


Fig. 6. Time series of the interface energy spectrum for $g = 1.3 \times 10^{10} g_{Earth}$. k_m and k_c are labelled for reference.

of microscale fluctuations, and therefore should not be expected to depend on gravity. At higher values of k , $\Delta n(k)$ becomes difficult to estimate accurately due to the magnitude of the fluctuations present.

The fact that $\Delta n(k)$ is an increasing function is in agreement with our expectation that $\Delta n(k) \rightarrow 0$ as we approach the macroscopic limit of small k . In other words, the single-run growth rates should converge to those predicted by continuum theory as the size of the system becomes large and the value of g becomes small.

Finally, it is instructive to examine the time evolution of the energy spectrum of the interface. A representative example is shown in Figure 6. The development of the interface is initially dominated by thermal fluctuations, as indicated by the approximately constant (i.e. white noise) early-time spectrum. At later times, the logarithms of the energy spectra are roughly evenly-spaced at evenly-spaced intervals of time, as expected for exponential growth. Furthermore, the peak of the later-time spectra clearly resides in the vicinity of the theoretical maximum k_m .

6 Conclusion

The results of this work provide further evidence that relatively small MD simulations are capable of successfully reproducing fluid flows as predicted by continuum models. The expected fluid behavior emerges as the ensemble mean of the microscopic flow, although individual instances of the flow may exhibit substantial deviations from NS-like behavior. The implication is that MD can describe fluids at all accessible length scales, including those at which deterministic, continuum models break down. Furthermore, this is the first work of which we are aware in which the

convergence of the mean of microscale fluctuations to the corresponding macroscopic, continuum limit has been investigated quantitatively (see Fig. 5).

As computational capacity continues to expand, MD and other atomistic methods will be increasingly able to accurately simulate complex flows at larger and larger scales. Works such this one are essential to the understanding of flow at small scales, and underscore the connection between micro- and macroscale models. The results of even small MD simulations may also have relevance to larger scales, as even a well-designed experiment will not be entirely free of external fluctuations.

We would like to thank E.G. Flekkøy, B.L. Holian, P.S. Lomdahl, and D. Livescu for valuable discussions, and the Institutional Computing Program at Los Alamos for supercomputer access. This work was supported by Department of Energy grant LDRD-20050066DR, and was carried out under the auspices of the National Nuclear Security Administration of the US Department of Energy at Los Alamos National Laboratory under Contract No. DE-AC52-06NA25396.

References

1. M. Moseler, U. Landman, *Science* **289**, 1165 (2000)
2. W.E. Alley, B.J. Alder, *Phys. Rev. A* **27**, 3158 (1983)
3. J.H. Irving, J.G. Kirkwood, *J. Chem. Phys.* **18**, 817 (1950)
4. M. Mareschal, E. Kestemont, *Nature* **329**, 427 (1987)
5. D.C. Rapaport, *Phys. Rev. E* **73**, 025301(R) (2006)
6. B.J. Alder, T. Wainwright, *J. Chem. Phys.* **27**, 1208 (1957)
7. M. Allen, D. Tildesley, *Computer Simulation of Liquids* (Oxford Science Publications, Oxford, 1987)
8. A. Lord Rayleigh, *Proc. London Math. Soc.* **14**, 170 (1883)
9. G.I. Taylor, *Proc. R. Soc. London Ser. A* **201**, 192 (1950)
10. G. Dimonte et al., *Phys. Fluids* **16**, 1668 (2004)
11. K. Kadau, T.C. Germann, N.G. Hadjiconstantinou, P.S. Lomdahl, G. Dimonte, B.L. Holian, B.J. Alder, *Proc. Nat. Acad. Sci.* **101**, 5851 (2004)
12. K. Kadau, C. Rosenblatt, J.L. Barber, T.C. Germann, Z. Huang, P. Carlès, B.J. Alder, *Proc. Nat. Acad. Sci.* **104**, 7741 (2007)
13. P. Carlès, Z. Huang, G. Carbone, C. Rosenblatt, *Phys. Rev. Lett.* **96**, 104501 (2006)
14. W.J. Harrison, *Proc. London Math. Soc.* **6**, 396 (1908)
15. S. Chandrasekhar, *Hydrodynamic and Hydromagnetic Stability* (Dover, New York, 1961)
16. E.G. Flekkøy, *Phys. Rev. Lett.* **75**, 260 (1995)
17. *CRC Handbook of Chemistry and Physics*, edited by D.R. Lide, 75th edn. (CRC Press, 1994)
18. P.S. Lomdahl, P. Tamayo, N. Gronbech-Jensen, D.M. Beazley, in *Proceedings of Supercomputing 93*, edited by G. S. Ansell (IEEE Computer Society Press, Los Alamitos, 1993), p. 520
19. D.M. Beazley, P.S. Lomdahl, *Comput. Phys.* **11**, 230 (1997)
20. D. Livescu, *Phys. Fluids* **16**, 118 (2004)